ACS APPLIED MATERIALS & INTERFACES

Research Article

www.acsami.org

Regulated Synthesis of Mo Sheets and Their Derivative MoX Sheets (X: P, S, or C) as Efficient Electrocatalysts for Hydrogen Evolution Reactions

Jin Jia,[†] Weijia Zhou,*[,†,‡] Guixiang Li,[†] Linjing Yang,[†] Zhaoqian Wei,[†] Lindie Cao,[†] Yisheng Wu,[†] Kai Zhou,[†] and Shaowei Chen*[,†,§]

[†]New Energy Research Institute, School of Environment and Energy, South China University of Technology, Guangzhou Higher Education Mega Center, Guangzhou, Guangdong 510006, China

[‡]Guangdong Provincial Key Laboratory of Atmospheric Environment and Pollution Control, South China University of Technology, Guangzhou Higher Education Mega Centre, Guangzhou, Guangdong 510006, China

[§]Department of Chemistry and Biochemistry, University of California, 1156 High Street, Santa Cruz, California 95064, United States

Supporting Information

ABSTRACT: Electrochemical H_2 generation from H_2O has been focused on the exploration of non-noble metals as well as earth-rich catalysts. In our practical work, we provide a simple cost-efficient fabrication process to prepare large Mo sheets via the controlled equilibrium between sublimation of MoO_3 and reduction of H_2. Porous MoP sheets were synthesized from the obtained Mo sheets as the Mo source and template which exhibit notable activity in the hydrogen evolution reaction with a low onset potential of −88 mV vs RHE, small Tafel value of 54.5 mV/dec, and strong catalytic stability. With Mo sheets as the universal Mo source and template, MoS_2 and Mo_2C sheets were synthesized by a similar process, and the corresponding catalytic activities were calculated by density functional theory.

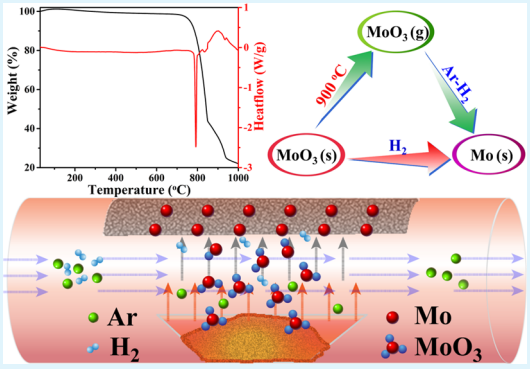

KEYWORDS: *Mo sheet, derivative MoX sheet, sublimation, catalytic site, hydrogen evolution reaction*

1. INTRODUCTION

Studies on electrochemical reduction of water to yield H_2 have been done due to the growing need for renewable and sustainable energy supplies.[1−6] H_2 serves as a renewable energy carrier and is nonpareil for fossil fuels in terms of its potential to ensure energy security and environmental friendliness.[7,8] To promote the hydrogen evolution reaction (HER), highly efficient electrocatalysts are thus essential. Nowadays, second to none of the HER catalysts with the highest efficiency are platinum (Pt) and Pt-based catalysts;[9−11] however, their large-scale applications have been restricted due to its scarcity and high price. Thus, development of efficient and cost-effective non-Pt HER electrocatalysts is highly desirable. During the past decades, various Mo precursors were employed to synthesize Mo-based electrocatalysts with tunable HER performance such as molybdenum sulfides,[12−20] phosphides,[21−23] carbides,[24−26] and nitrides.[27−30] For example, Cui's group[31] reported a synthesis method to grow vertically aligned MoS_2 and $MoSe_2$ layers on the surface of Mo bulk metal. However, Mo bulk metal possesses limited electrochemical area, which caused poor HER activity coupling with the overpotential of 300 mV vs RHE to realize a current density of 0.5 mA/cm^2. Therefore, how to increase the electrochemical area of electrocatalysts to obtain a large current density for HER is a worthy problem.

Here, we report the scalable synthesis of Mo sheets by combining the sublimation of MoO_3 and reduction of Ar−H_2 (10%) mixture gas at 900 °C. The sublimation reaction of MoO_3 being utilized as a template to synthesize various hollow shell structures is widely reported.[32,33] Herein, the obtained Mo sheets were used as the Mo source and template to synthesize Mo-based electrocatalysts such as molybdenum phosphide (MoP) sheets, which is a typical transition metal phosphide with prominent catalytic activity and outstanding stability for HER.[22,23,34,35] The obtained MoP sheets as a vigorous HER electrocatalyst exhibited commendable activity with a small onset potential of −88 mV vs RHE, low Tafel slope of 54.5 mV/dec, and robust stability (over 21 h of incessant working at −250 mV vs RHE). Moreover, other molybdenum compound sheets such as MoS_2 and Mo_2C were also derived from Mo sheets, which possessed high catalytic activity for HER.

2. EXPERIMENTAL SECTION

2.1. Materials. Analytical grade ammonium molybdate ($(NH_4)_6Mo_7O_{24}{\cdot}4H_2O$), molybdenum powder (Mo), sodium hypo-

Received: September 23, 2016
Accepted: February 16, 2017
Published: February 16, 2017

DOI: 10.1021/acsami.6b12103
ACS Appl. Mater. Interfaces 2017, 9, 8041−8046

phosphite (NaH_2PO_2), thioacetamide (CH_3CSNH_2), methane (CH_4), and 20 wt % Pt/C were purchased from Sinopharm Chemical Reagents Beijing Co. and used without further purification.

2.2. Synthesis of Mo Sheets and Mo Particles. The purchased ammonium molybdate was calcined for 4 h at 550 °C under air atmosphere to obtain MoO_3 precursors. Growth of Mo sheets on the quartz tube wall was performed inside a tubular furnace. MoO_3 powders in a porcelain crucible were positioned at the center of the quartz tube. Ar gas (100 mTorr) was pumped into the quartz tube to remove air. Subsequently, the MoO_3 powders were quickly heated from room temperature to 900 °C (20 °C/min) and maintained at 900 °C for 4 h under an Ar−H_2 (10%) mixture gas flow of 100 sccm. After the reaction, the gray Mo sheets were collected from the porcelain crucible and/or inside wall of the quartz tube. Mo particles were obtained from the bottom of the porcelain boat by using pure H_2 instead of Ar−H_2 (10%).

2.3. Synthesis of MoP Sheets and MoP Particles. One gram of NaH_2PO_2 particles in the front of Mo sheets or particles was mildly decomposed at ~250 °C with heating belts and transported by Ar gas (10 sccm) toward the downstream hot zone. As-prepared Mo sheets or particles were rapidly heated to 900 °C (20 °C/min), which was maintained for 1 h. After that, Ar gas was kept flowing (50 sccm) to remove residue phosphine. The effect of calcination temperature (700, 800, 900, 1000 °C) was considered, which resulted in inconspicuous changes in HER performance of MoP sheets (Figure S1). To confirm the universality, Mo sheets as an alternative Mo source and template were used to synthesize MoS_2 and Mo_2C sheets by subsequent sulphurization and carbonization process, respectively, as shown in the Supporting Information. Detailed information about characterization, electrochemistry, and density functional theory (DFT) calculations are also in the Supporting Information.

3. RESULTS AND DISCUSSION

Formation of Mo sheets in the tube furnace is schematically illustrated in Scheme 1, also photos of different products and

Scheme 1. (a) TGA-DSC Curves of MoO_3 Powders from Room Temperature to 1000 °C in an Oxygen Atmosphere, (b) Schematic Diagram of Reaction Relation among MoO_3 (Solid), MoO_3 (Gas) and Mo (Solid), and (c) Atomic Structure Diagram of Reaction Relation at 900 °C under Ar−H_2 (10%)

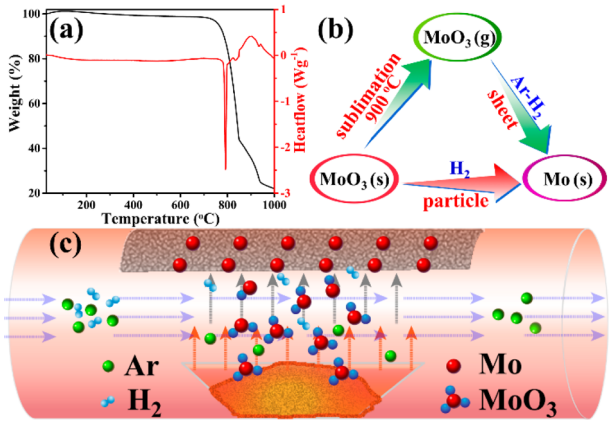

corresponding collect positions are summarized in Figure 1. There is an equilibrium between sublimation of MoO_3 and reduction by gas mixture of Ar−H_2 (10%). The sublimation temperature of MoO_3 (corresponding scanning electron microscopy (SEM) images and X-ray diffraction (XRD) results are shown in Figure S2) was identified as 790 °C by thermal gravimetric analysis-differential scanning calorimetry (TGA-DSC, Scheme 1a). The volatile suboxide species of MoO_{3-x} sublimated from MoO_3 powder at 900 °C were reduced into Mo sheets by Ar−H_2 (10%) on the quartz tube wall (Scheme 1 and Figure 1a, corresponding SEM images and XRD results are in Figure 2). To confirm the reaction mechanism, pure H_2 gas with stronger reduction features was used instead of Ar−H_2 (10%). Only large Mo particles at the bottom of porcelain crucible were obtained, and no Mo sheets were synthesized on the quartz tube wall (Figures 1b and S3). In addition, no Mo sheets were synthesized at 650 °C, lower than the sublimation temperature of MoO_3 on the quartz tube wall, and only MoO_2 particles were obtained at the bottom of porcelain crucible (Figure 1c, corresponding SEM images and XRD results in Figure S4). Therefore, controlled equilibrium between sublimation of MoO_3 and reduction of H_2 is critical to obtain Mo sheets. It is worth noting that the obtained Mo sheets were fluffy, and the volume of the quality (0.15 g) was much larger than those of MoO_3 (1.5 g), MoO_2 (1.5 g), and Mo (1.5 g) powders (Figure S5), which was consistent with Brunauer−Emmett−Teller (BET) results. The BET value of Mo sheets (5.504 m^2/g, Figure S6) calculated by N_2 adsorption−desorption isotherms was much larger than those of MoO_3 (0.706 m^2/g) and Mo (0.709 m^2/g) powders. Herein, the Mo sheets as an alternative Mo source and template were used to synthesize various molybdenum compounds such as MoP, MoS_2, and Mo_2C sheets by subsequent phosphating, sulphurization, and carbonization processes, respectively.

SEM was implemented to examine the morphologies and structures of as-synthesized Mo and MoP sheets. Figures 2a and b showed that the as-synthesized Mo sheets possessed a smooth surface with size of 2−10 μm and thickness of 50−100 nm. The Mo sheets possessed the dendritic slices due to the metastable state of Mo during equilibrium between sublimation of MoO_3 and reduction of Ar−H_2 (10%) at high temperature. After phosphorization, the obtained MoP sheets with convex−concave surface were composed of a large number of small MoP nanoparticles (Figures 2c and d), and the thickness increased to 100−200 nm. The successful syntheses of Mo (PDF no. 42-1120) and MoP (PDF no. 24-0771) with perfect crystallization peaks were confirmed by XRD, and no impurities were detected (Figure 2e). Figure S7 presented the corresponding EDS Mo and P elemental mapping images for MoP sheets, evidently showing that two elements are uniformly dispersed in the whole sheets. X-ray photoelectron spectroscopy (XPS) determined the exterior elemental composition of the as-made materials. The Mo 3d spectrum of Mo sheets exhibited three peaks at 235, 232, and 228 eV that were attributed to Mo^{6+} $3d_{3/2}$, Mo^{4+} $3d_{5/2}$, and Mo^{4+} $3d_{3/2}$, respectively (Figure 2f). No zerovalent Mo was detected by the surface testing technique of XPS due to surface oxidation of Mo sheets via exposure to air.[21] However, the oxidation layer of Mo sheets was too thin, which was not detected by XRD. In addition, the two peaks at 227.8 and 231 eV in the Mo 3d spectrum of MoP sheets were assigned to the Mo^{3+} within MoP sheets. The peaks at 129.1 and 129.9 eV for MoP sheets were assigned to P $2p_{1/2}$ and P $2p_{3/2}$ bonded to Mo, respectively (Figure 2g). One weak peak at 133.5 eV was assigned to PO_4^{3-}, which was consistent with reported results.[22,36]

Transmission electron microscopy (TEM) measurements were performed to further characterize the morphologies and crystal structure of Mo and MoP sheets. As shown in Figure 3a, Mo sheets are mainly lamellar and dendritic slices. Note that only the long-range crystalline lattices of 0.222 nm were observed in Mo sheets (Figure 3b), corresponding to (110) of

DOI: 10.1021/acsami.6b12103
ACS Appl. Mater. Interfaces 2017, 9, 8041−8046

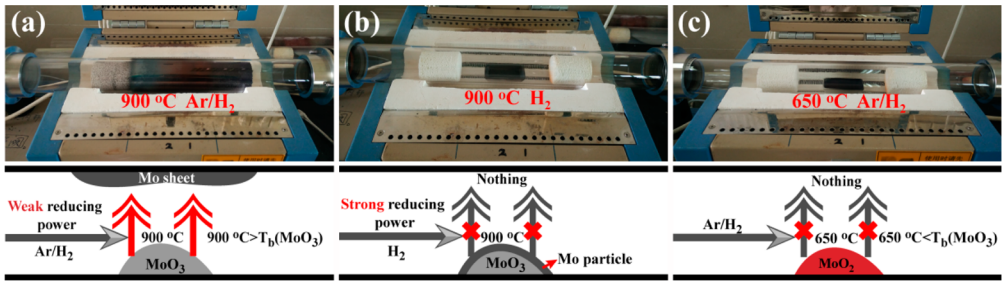

Figure 1. Collect positions and schematic illustration of (a) Mo sheets prepared at 900 °C under Ar−H_2 (10%) atmosphere, (b) Mo particles prepared at 900 °C under H_2 atmosphere, and (c) MoO_2 particles prepared at 650 °C under Ar−H_2 (10%) atmosphere.

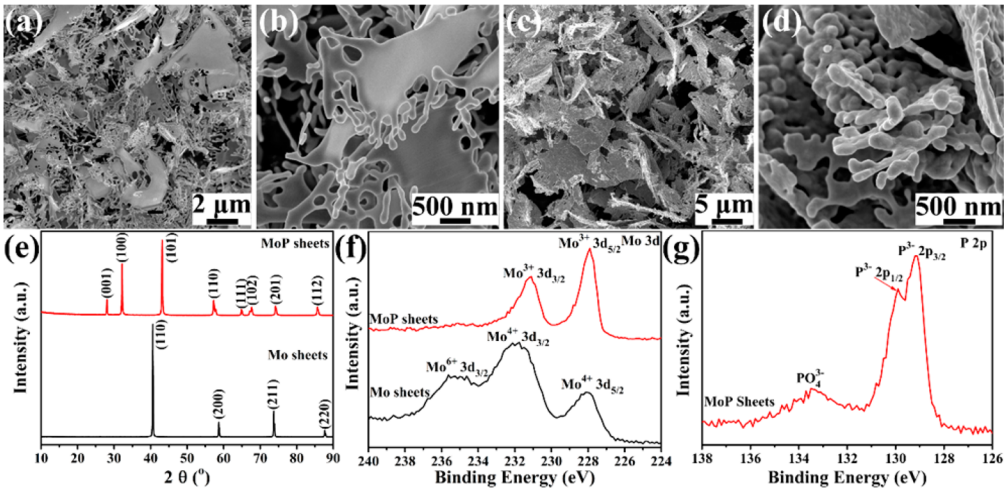

Figure 2. SEM images of (a and b) Mo sheets and (c and d) MoP sheets, (e) XRD patterns of Mo sheets and corresponding MoP sheets, and XPS spectra of (f) Mo and (g) P of MoP sheets and Mo sheets.

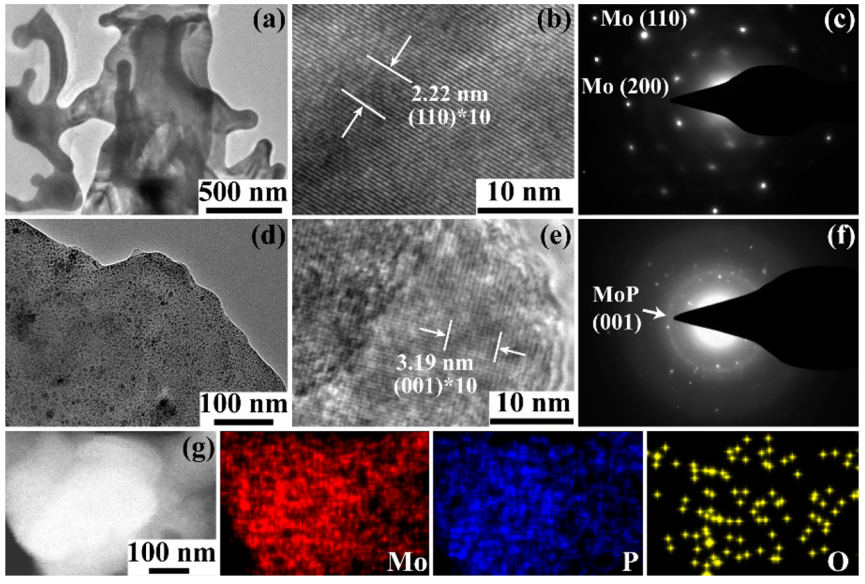

Figure 3. TEM images, SAED pattern of (a−c) Mo sheets and (d−f) MoP sheets, and (g) EDX mapping of the MoP sheet.

body-centered cubic (bcc) Mo. Consistent behaviors were observed in the selected area electron diffraction (SAED) measurements (Figure 3c), and the regular arrangement of scattered dots suggested single-crystal Mo sheets. After phosphorization, the coarse sheets were composed of MoP nanoparticles, and crystalline lattices of 0.319 nm corresponded to the (001) plane of MoP (Figure 3d, e). The diffraction rings in the SAED pattern were indexed to the (101) plane of MoP (Figure 3f), suggesting the phase transformation from single-crystal Mo sheets to polycrystalline MoP sheets. Energy-dispersive X-ray (EDX) elemental mapping of a selected MoP sheet shows that the Mo and P elements were indeed uniformly distributed in the sheet yet had sparsely distributed O signals (Figure 3g).

DOI: 10.1021/acsami.6b12103
ACS Appl. Mater. Interfaces 2017, 9, 8041−8046

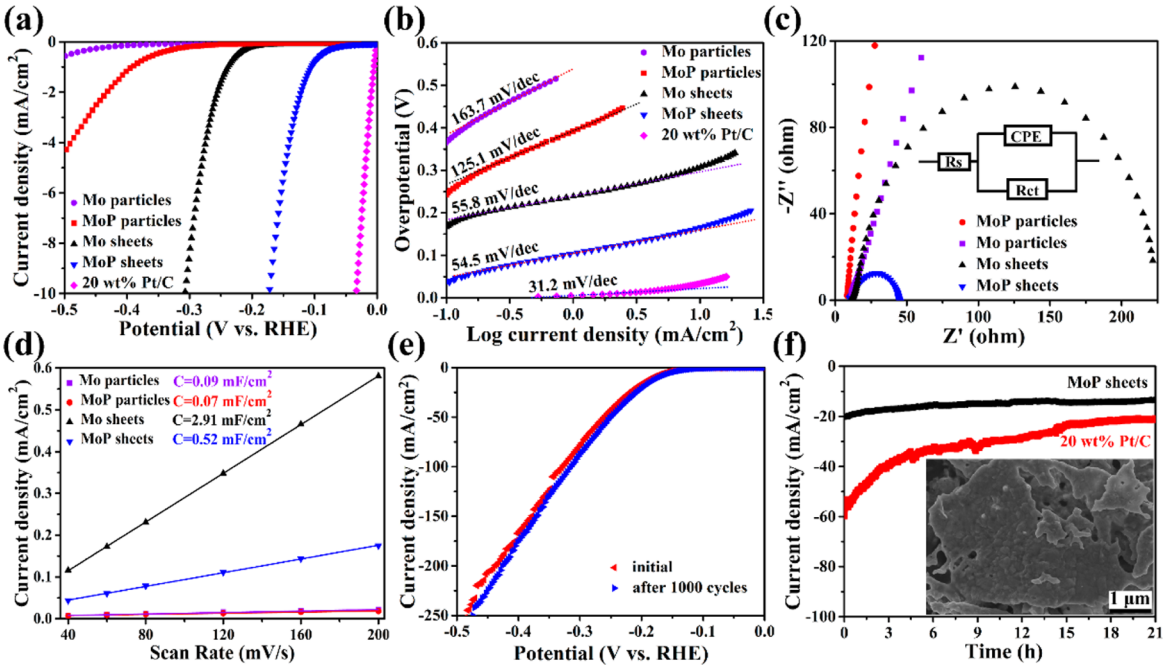

Figure 4. (a) Polarization curves of Mo particles, MoP particles, Mo sheets, MoP sheets, and 20 wt % Pt/C at 5 mV/s in a 0.5 M H_2SO_4 (*iR*-uncorrected) and (b) Tafel plots calculated from panel a. (c) Electrochemical impedance spectra of various samples for HER with overpotential of 250 mV. (d) Variation in electrochemical active area with potential scan rate. (e) Polarization curves of MoP sheets before and after 1000 cycles. (f) The *i*−*t* testing curve of MoP sheets and 20 wt % Pt/C loaded on carbon cloth at −0.25 V vs RHE for 21 h. Inset is the SEM image of MoP sheets after *i*−*t* testing.

The electrocatalytic activities of MoP sheets and blank samples, including Mo particles, MoP particles, Mo sheets, and 20 wt % Pt/C for HER, were investigated by a three-electrode configuration. Figure 4a shows that MoP sheets exhibited a much lower onset potential of −88 mV vs RHE (achieve to 0.5 mA/cm^2) compared to those of Mo sheets (−223 mV), MoP particles (−353 mV), and Mo particles (−492 mV); however, it was still worse than that of 20 wt % Pt/C (∼0 mV). Moreover, for MoP sheet electrocatalysts, an overpotential of 172 mV was required to reach 10 mA/cm^2. In addition, commercial molybdenum powder (Figure S8a) was also used to synthesize MoP particles (Figure S8b), which possessed the worst HER performance compared to that of MoP sheets (Figure S9), confirming the advantage of Mo sheets synthesized via the controlled equilibrium between sublimation of MoO_3 and reduction of H_2.

The according Tafel slopes were also compared in Figure 4b, which were obtained via the Tafel equation. The Tafel slope of MoP sheets was 54.5 mV/dec, which was lower than those of other samples, including Mo sheets (55.8 mV/dec), Mo particles (163.7 mV/dec), and MoP particles (125.1 mV/dec), yet larger than that of 20 wt % Pt/C (31.2 mV/dec). On the basis of the HER mechanism, HER at MoP sheets likely proceeded through a Volmer−Heyrovsky mechanism with the rate-limiting step of the electrochemical discharge process. Beyond that, the exchange current densities of the Mo particles, MoP particles, Mo sheets, and MoP sheet electrocatalysts were calculated to be 0.3×10^{-3}, 1.0×10^{-3}, 5.6×10^{-3}, and 3.2×10^{-2} mA/cm^2, respectively (Figure S10). A lower Tafel slope and the larger exchange current density of MoP sheets indicated fast HER kinetics. Such an HER performance of MoP sheets (−88 mV vs RHE, 54.5 mV/dec, and exchange current density of 3.2×10^{-2} mA/cm^2) was comparable to those of some leading Mo-based electrocatalysts such as MoP nanoparticles (−125 mV, 74 mV/dec, 1.3×10^{-5} mA/cm^2),[23] MoP microparticles (−80 mV, 50 mV/dec, 1.0×10^{-2} mA/cm^2),[37] and MoP particles (−88 mV, 60 mV/dec, 4.1×10^{-3} mA/cm^2),[38] as shown in Table S1. In addition, MoP sheets had the ability to be operated in 0.5 M H_2SO_4 (pH 0.25), 1 M phosphate buffer (pH 7), and 1 M KOH (pH 14), as shown in Figure S11.

Electrochemical impedance spectroscopy measurements were promptly executed to determine the involved electron transfer kinetics in HER. Figure 4c depicts the Nyquist plots acquired with an overpotential of 250 mV for glassy carbon electrodes modified with the various catalyst samples. The MoP sheets exhibited a charge transfer resistance (R_{ct}) smaller than that of other samples, as manifested by the smallest semicircle, consistent with the best HER performance. In addition, R_{ct} actually diminished from 253 Ω at −150 mV to 45 Ω at −250 mV, as depicted in Figure S12, suggesting the favorable charge transfer at the interface between electrolyte and electrodes.

Typically, the catalytically active surface area of electrocatalysts is proportional to the catalytic current density and can be measured by the double layer capacitance. The double layer capacitance of MoP sheets (0.52 mF/cm^2) was less than that of Mo sheets (2.91 mF/cm^2) but much larger than those of Mo particles (0.09 mF/cm^2) and MoP particles (0.07 mF/cm^2), as shown in Figures 4d and S13. The electrochemical active area of MoP sheets was small due to the high Mo atomic weight, consistent with the low BET surface area value of ∼4.1 m^2/g (Figure S6).

The extraordinary HER stability of the electrocatalyst was also crucial, as was catalytic activity for HER. Figure 4e depicts the polarization curves of MoP sheets before and after 1000 cycles, where a negligible decrease in the current density was observed. Moreover, over 21 h of continuous *i*−*t* testing at −0.25 V vs RHE, the current density of MoP sheets had a

DOI: 10.1021/acsami.6b12103
ACS Appl. Mater. Interfaces 2017, 9, 8041−8046

negligible change, confirming the remarkable HER stability (Figure 4f). The inset of Figure 4f confirms that the MoP sheets possessed good structural stability as well as catalytic stability after *i*−*t* testing. As a comparison, 20 wt % Pt/C was also operated at the same potential and time; the current density changed greatly from 60 to 21 mA/cm^2, which was reduced by about 65%. At last, the gathered bubbles on MoP sheet-modified electrode were established to be H_2 through gas chromatography analysis, and the corresponding H_2 generation rate was 619.2 mmol/g/h (Figure S14).

To confirm that the Mo sheet can be used as a universal Mo source and template, the MoS_2 and Mo_2C sheets were also synthesized by a similar process. The SEM images, XRD, and XPS results of the obtained MoS_2 and Mo_2C sheets are shown in Figure S15. After sulphurization and carbonization, the sheet morphologies remained, but the surface was rough due to the formation of MoS_2 and Mo_2C nanoparticles. The HER electrocatalytic activities of MoS_2 and Mo_2C sheets were subsequently studied (Figure S16), which possessed small overpotentials of 215 and 223 mV required to arrive at the current density of 10 mA/m^2, respectively. In addition, the catalytic active sites of MoP, MoS_2, and Mo_2C were investigated by DFT calculations (Figure 5). The DFT

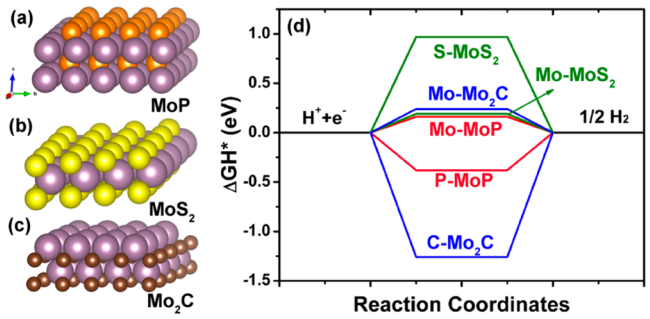

Figure 5. Structural models of (a) MoP, (b) MoS_2, and (c) Mo_2C and (d) Gibbs free energy of H* adsorption (ΔGH^*) profile for various sites.

calculation was focused on the Gibbs free energy changes of hydrogen absorbed onto different active sites, which was an important intermediate state in HER. According to the Sabatier principle, too weak or too strong adsorption was unfavorable for the catalyst reaction. It can be seen from the calculations that the hydrogen atom always had a Gibbs free energy (ΔGH^*) that was closer to zero on Mo atoms terminated with MoP (0.16 eV), MoS_2 (0.19 eV), and Mo_2C (0.24 eV), indicating that the active sites prefer the Mo atom (Figure 5d). The results also showed that P atoms (−0.38 eV) had a role equivalent to that of S atoms (0.97 eV) in MoS_2 and C atoms (−1.26 eV) in Mo_2C, which took responsibility for constructing large quantities of active edges for HER. As shown in Figure 5d, Mo active sites in MoP gave a ΔGH^* value subtly smaller than those of MoS_2 and Mo_2C sheets, indicating that MoP possessed a higher catalytic activity for HER, which was in approximate accordance with the experimental analysis and results. Here, it is clear that these above-mentioned results effectively confirmed that the Mo sheets were an efficient template to synthesize Mo-based electrocatalysts with efficient catalytic performance.

4. CONCLUSIONS

Herein, we reported a novel approach to synthesize MoP via the use of Mo sheets which were obtained by the controlled equilibrium between sublimation of MoO_3 and reduction of H_2. While the MoP sheets as electrocatalysts possessed high HER activities (−88 mV vs RHE, 54.5 mV/dec, and exchange current density of 3.2×10^{-2} mA/cm^2), they also had benign structural and catalytic stability, which is much better than that of MoP particles. In addition, Mo sheets as a universal Mo source and template were used to synthesize MoS_2 and Mo_2C sheets by a similar process, and the catalytic active sites of MoP, MoS_2, and Mo_2C were investigated by DFT calculations. Further, the facile, large-volume, low-cost synthetic technology of Mo sheets may enlighten a new avenue to extensively produce the Mo-based electrocatalysts with sheet structures.

■ ASSOCIATED CONTENT

Supporting Information

The Supporting Information is available free of charge on the ACS Publications website at DOI: 10.1021/acsami.6b12103.

Experimental section of MoS_2 and Mo_2C sheets; detailed information about characterization, electrochemistry, and DFT calculations; comparison of HER performance among MoP particles; SEM images and XRD results of MoO_3, MoO_2, Mo, and MoP particles; photo of 1.5 g of MoO_3 particles, 1.5 g of MoO_2 particles, 1.5 g of Mo particles, and 0.15 g of Mo sheets; exchange current density and cyclic voltammograms; polarization curves for HER in 1 M KOH (pH 14) and 1 M phosphate buffer (pH 7), Nyquist plots and the amount of hydrogen production of MoP sheets; and SEM, XRD, XPS, Tafel plots, and polarization curves of Mo_2C and MoS_2 sheets in 0.5 M H_2SO_4 (PDF)

■ AUTHOR INFORMATION

Corresponding Authors

* E-mail: eszhouwj@scut.edu.cn.
*E-mail: shaowei@ucsc.edu.

ORCID

Weijia Zhou: 0000-0003-4339-0435
Shaowei Chen: 0000-0002-3668-8551

Notes

The authors declare no competing financial interest.

■ ACKNOWLEDGMENTS

This work was supported by the National Recruitment Program of Global Experts, Project of Public Interest Research and Capacity Building of Guangdong Province (Grant no. 2014A010106005), the National Natural Science Foundation of China (Grant no. 51502096), and the Guangdong Innovative and Entrepreneurial Research Team Program (Grant no. 2014ZT05N200).

■ REFERENCES

(1) Zhou, W.; Wu, X. J.; Cao, X.; Huang, X.; Tan, C.; Tian, J.; Liu, H.; Wang, J.; Zhang, H. Ni_3S_2 Nanorods/Ni Foam Composite Electrode with Low Overpotential for Electrocatalytic Oxygen Evolution. *Energy Environ. Sci.* **2013**, *6*, 2921−2924.
(2) Zou, X.; Zhang, Y. Noble Metal-free Hydrogen Evolution Catalysts for Water Splitting. *Chem. Soc. Rev.* **2015**, *44*, 5148−5180.

DOI: 10.1021/acsami.6b12103
ACS Appl. Mater. Interfaces 2017, 9, 8041−8046

(3) Vesborg, P. C.; Seger, B.; Chorkendorff, I. Recent Development in Hydrogen Evolution Reaction Catalysts and Their Practical Implementation. *J. Phys. Chem. Lett.* **2015**, *6*, 951−957.
(4) Zhou, W.; Jia, J.; Lu, J.; Yang, L.; Hou, D.; li, G.; Chen, S. Recent Developments of Carbon-based Electrocatalysts for Hydrogen Evolution Reaction. *Nano Energy* **2016**, *28*, 29−43.
(5) Pu, Z.; Wei, S.; Chen, Z.; Mu, S. Flexible Molybdenum Phosphide Nanosheet Array Electrodes for Hydrogen Evolution Reaction in a Wide pH Range. *Appl. Catal., B* **2016**, *196*, 193−198.
(6) Zhou, W.; Xiong, T.; Shi, C.; Zhou, J.; Zhou, K.; Zhu, N.; Li, L.; Tang, Z.; Chen, S. Bioreduction of Precious Metals by Microorganism: Efficient Gold@N-Doped Carbon Electrocatalysts for the Hydrogen Evolution Reaction. *Angew. Chem., Int. Ed.* **2016**, *55*, 8416−8420.
(7) Cook, T. R.; Dogutan, D. K.; Reece, S. Y.; Surendranath, Y.; Teets, T. S.; Nocera, D. G. Solar Energy Supply and Storage for the Legacy and Nonlegacy Worlds. *Chem. Rev.* **2010**, *110*, 6474−6502.
(8) Walter, M. G.; Warren, E. L.; McKone, J. R.; Boettcher, S. W.; Mi, Q.; Santori, E. A.; Lewis, N. S. Solar Water Splitting Cells. *Chem. Rev.* **2010**, *110*, 6446−6473.
(9) Subbaraman, R.; Tripkovic, D.; Strmcnik, D.; Chang, K. C.; Uchimura, M.; Paulikas, A. P.; Stamenkovic, V.; Markovic, N. M. Enhancing Hydrogen Evolution Activity in Water Splitting by Tailoring Li^+-$Ni(OH)_2$-Pt Interfaces. *Science* **2011**, *334*, 1256−1260.
(10) Li, M.; Ma, Q.; Zi, W.; Liu, X.; Zhu, X.; Liu, S. F. Pt Monolayer Coating on Complex Network Substrate with High Catalytic Activity for the Hydrogen Evolution Reaction. *Sci. Adv.* **2015**, *1*, e1400268.
(11) Greeley, J.; Jaramillo, T. F.; Bonde, J.; Chorkendorff, I.; Nørskov, J. K. Computational High-throughput Screening of Electrocatalytic Materials for Hydrogen Evolution. *Nat. Mater.* **2006**, *5*, 909−913.
(12) Lukowski, M. A.; Daniel, A. S.; Meng, F.; Forticaux, A.; Li, L.; Jin, S. Enhanced Hydrogen Evolution Catalysis from Chemically Exfoliated Metallic MoS_2 Nanosheets. *J. Am. Chem. Soc.* **2013**, *135*, 10274−10277.
(13) Xie, J.; Zhang, J.; Li, S.; Grote, F.; Zhang, X.; Zhang, H.; Wang, R.; Lei, Y.; Pan, B.; Xie, Y. Controllable Disorder Engineering in Oxygen-incorporated MoS_2 Ultrathin Nanosheets for Efficient Hydrogen Evolution. *J. Am. Chem. Soc.* **2013**, *135*, 17881−17888.
(14) Xie, J.; Zhang, H.; Li, S.; Wang, R.; Sun, X.; Zhou, M.; Zhou, J.; Lou, X. W.; Xie, Y. Defect-rich MoS_2 Ultrathin Nanosheets with Additional Active Edge Sites for Enhanced Electrocatalytic Hydrogen Evolution. *Adv. Mater.* **2013**, *25*, 5807−5813.
(15) Zhou, W. J.; Hou, D. M.; Sang, Y. H.; Yao, S. H.; Zhou, J.; Li, G. Q.; Li, L. G.; Liu, H.; Chen, S. W. MoO_2 Nanobelts@nitrogen Self-doped MoS_2 Nanosheets as Effective Electrocatalysts for Hydrogen Evolution Reaction. *J. Mater. Chem. A* **2014**, *2*, 11358−11364.
(16) Zhou, W.; Zhou, K.; Hou, D.; Liu, X.; Li, G.; Sang, Y.; Liu, H.; Li, L.; Chen, S. Three-dimensional Hierarchical Frameworks Based on MoS_2 Nanosheets Self-assembled on Graphene Oxide for Efficient Electrocatalytic Hydrogen Evolution. *ACS Appl. Mater. Interfaces* **2014**, *6*, 21534−21540.
(17) Yang, L.; Zhou, W.; Hou, D.; Zhou, K.; Li, G.; Tang, Z.; Li, L.; Chen, S. Porous Metallic MoO_2-supported MoS_2 Nanosheets for Enhanced Electrocatalytic Activity in the Hydrogen Evolution Reaction. *Nanoscale* **2015**, *7*, 5203−5208.
(18) Xie, J.; Xie, Y. Structural Engineering of Electrocatalysts for the Hydrogen Evolution Reaction: Order or Disorder? *ChemCatChem* **2015**, *7*, 2568−2580.
(19) Yang, L.; Zhou, W.; Lu, J.; Hou, D.; Ke, Y.; Li, G.; Tang, Z.; Kang, X.; Chen, S. Hierarchical Spheres Constructed by Defect-rich MoS_2/carbon Nanosheets for Efficient Electrocatalytic Hydrogen Evolution. *Nano Energy* **2016**, *22*, 490−498.
(20) Xie, J.; Xin, J.; Cui, G.; Zhang, X.; Zhou, L.; Wang, Y.; Liu, W.; Wang, C.; Ning, M.; Xia, X. Vertically Aligned Oxygen-doped Molybdenum Disulfide Nanosheets Grown on Carbon Cloth Realizing Robust Hydrogen Evolution Reaction. *Inorg. Chem. Front.* **2016**, *3*, 1160−1166.
(21) Xiao, P.; Sk, M. A.; Thia, L.; Ge, X.; Lim, R. J.; Wang, J. Y.; Lim, K. H.; Wang, X. Molybdenum Phosphide as an Efficient Electrocatalyst for the Hydrogen Evolution Reaction. *Energy Environ. Sci.* **2014**, *7*, 2624−2629.
(22) Kibsgaard, J.; Jaramillo, T. F. Molybdenum phosphosulfide: an Active, Acid-stable, Earth-abundant atalyst for the Hydrogen Evolution Reaction. *Angew. Chem., Int. Ed.* **2014**, *53*, 14433−14437.
(23) Yang, J.; Zhang, F.; Wang, X.; He, D.; Wu, G.; Yang, Q.; Hong, X.; Wu, Y.; Li, Y. Porous Molybdenum Phosphide Nano-Octahedrons Derived from Confined Phosphorization in UIO-66 for Efficient Hydrogen Evolution. *Angew. Chem.* **2016**, *128*, 13046−13050.
(24) Ma, F. X.; Wu, H. B.; Xia, B. Y.; Xu, C. Y.; Lou, X. W. Hierarchical beta-Mo_2C Nanotubes Organized by Ultrathin Nanosheets as a Highly Efficient Electrocatalyst for Hydrogen Production. *Angew. Chem., Int. Ed.* **2015**, *54*, 15395−15399.
(25) Li, C. J.; Wang, S. P.; Wang, T.; Wei, Y. J.; Zhang, P.; Gong, J. L. Monoclinic Porous $BiVO_4$ Networks Decorated by Discrete g-C_3N_4 Nano-Islands with Tunable Coverage for Highly Efficient Photocatalysis. *Small* **2014**, *10*, 2783−2790.
(26) Wu, H. B.; Xia, B. Y.; Yu, L.; Yu, X. Y.; Lou, X. W. Porous Molybdenum Carbide Nano-octahedrons Synthesized via Confined Carburization in Metal-organic Frameworks for Efficient Hydrogen Production. *Nat. Commun.* **2015**, *6*, 6512.
(27) Chen, W. F.; Sasaki, K.; Ma, C.; Frenkel, A. I.; Marinkovic, N.; Muckerman, J. T.; Zhu, Y.; Adzic, R. R. Hydrogen-evolution Catalysts based on Non-noble Metal Nickel-molybdenum Nitride Nanosheets. *Angew. Chem., Int. Ed.* **2012**, *51*, 6131−6135.
(28) Xie, J.; Li, S.; Zhang, X.; Zhang, J.; Wang, R.; Zhang, H.; Pan, B.; Xie, Y. Atomically-thin Molybdenum Nitride Nanosheets with Exposed Active Surface Sites for Efficient Hydrogen Evolution. *Chem. Sci.* **2014**, *5*, 4615−4620.
(29) Cao, B.; Veith, G. M.; Neuefeind, J. C.; Adzic, R. R.; Khalifah, P. G. Mixed close-packed Cobalt Molybdenum Nitrides as Non-noble Metal Electrocatalysts for the Hydrogen Evolution Reaction. *J. Am. Chem. Soc.* **2013**, *135*, 19186−19192.
(30) Xie, J.; Xie, Y. Transition Metal Nitrides for Electrocatalytic Energy Conversion: Opportunities and Challenges. *Chem. - Eur. J.* **2016**, *22*, 3588−3598.
(31) Kong, D.; Wang, H.; Cha, J. J.; Pasta, M.; Koski, K. J.; Yao, J.; Cui, Y. Synthesis of MoS_2 and $MoSe_2$ Films with Vertically Aligned Layers. *Nano Lett.* **2013**, *13*, 1341−1347.
(32) Qiu, J.; Yang, Z.; Li, Y. N-doped Carbon Encapsulated Ultrathin MoO_3 Nanosheets as Superior Anodes with High Capacity and Excellent Rate Capability for Li-ion Batteries. *J. Mater. Chem. A* **2015**, *3*, 24245−24253.
(33) Yang, X.; Li, Q.; Hu, G.; Wang, Z.; Yang, Z.; Liu, X.; Dong, M.; Pan, C. Controlled Synthesis of High-quality Crystals of Monolayer MoS_2 for Nanoelectronic Device Application. *Science China Materials* **2016**, *59*, 182−190.
(34) Wang, X. D.; Xu, Y. F.; Rao, H. S.; Xu, W. J.; Chen, H. Y.; Zhang, W. X.; Kuang, D. B.; Su, C. Y. Novel Porous Molybdenum Tungsten Phosphide Hybrid Nanosheets on Carbon Cloth for Efficient Hydrogen Evolution. *Energy Environ. Sci.* **2016**, *9*, 1468−1475.
(35) Liu, J.; Tang, S.; Lu, Y.; Cai, G.; Liang, S.; Wang, W.; Chen, X. Synthesis of Mo_2N Nanolayer Coated MoO_2 Hollow Nanostructures as High-performance Anode Materials for Lithium-ion Batteries. *Energy Environ. Sci.* **2013**, *6*, 2691−2697.
(36) Bai, J.; Li, X.; Wang, A.; Prins, R.; Wang, Y. Hydrodesulfurization of Dibenzothiophene and its Hydrogenated Intermediates over Bulk MoP. *J. Catal.* **2012**, *287*, 161−169.
(37) Wang, T.; Du, K.; Liu, W.; Zhu, Z.; Shao, Y.; Li, M. Enhanced Electrocatalytic Activity of MoP Microparticles for Hydrogen Evolution by Grinding and Electrochemical Activation. *J. Mater. Chem. A* **2015**, *3*, 4368−4373.
(38) Chen, X.; Wang, D.; Wang, Z.; Zhou, P.; Wu, Z.; Jiang, F. Molybdenum Phosphide: a New Highly Efficient Catalyst for the Electrochemical Hydrogen Evolution Reaction. *Chem. Commun.* **2014**, *50*, 11683−11685.

DOI: 10.1021/acsami.6b12103
ACS Appl. Mater. Interfaces 2017, 9, 8041−8046